SCIENCE CHINA
Information Sciences

• RESEARCH PAPER •
Special Focus on Photonics in AI

June 2020, Vol. 63 160408:1–160408:8
https://doi.org/10.1007/s11432-020-2887-6

Demonstration of a distributed feedback laser diode working as a graded-potential-signaling photonic neuron and its application to neuromorphic information processing

Bowen MA & Weiwen ZOU*

State Key Laboratory of Advanced Optical Communication Systems and Networks, Intelligent Microwave Lightwave Integration Innovation Center (iMLic), Department of Electronic Engineering, Shanghai Jiao Tong University, Shanghai 200240, China

Received 25 January 2020/Revised 28 March 2020/Accepted 22 April 2020/Published online 9 May 2020

Abstract We find that a commonly-used distributed feedback laser diode (DFB-LD) can work as a graded-potential-signaling photonic neuron. Through theoretical and experimental demonstration, DFB-LDs are proved useful for three graded-potential-signaling-based neuromorphic processing applications of the pattern recognition, the single-wavelength implementation of spike timing dependent plasticity (STDP), and the sound azimuth measurement. The pattern recognition with a full-width-at-half-maximum (FWHM) of 1 μs is realized in the experiment.

Keywords neuromorphic photonics, graded-potential-signaling photonic neuron, pattern recognition, optical spike timing dependent plasticity, sound azimuth measurement

Citation Ma B W, Zou W W. Demonstration of a distributed feedback laser diode working as a graded-potential-signaling photonic neuron and its application to neuromorphic information processing. Sci China Inf Sci, 2020, 63(6): 160408, https://doi.org/10.1007/s11432-020-2887-6

1 Introduction

Neuromorphic photonics, as a competitive candidate for the next-generation information processing system, is expected to achieve a brand-new framework by endowing the photonic platform with biological plausibility [1]. Neuromorphic photonics is hopeful owing to the pipelining nature of photonics with high speed, wide bandwidth, and low energy dissipation, while the electronic counterpart is bandwidth-limited and sensitive to the crosstalk [2–5]. Towards a neuromorphic photonic network and/or processor, a photonic neuron serves as a fundamental element to extract information from the high-density synaptic inputs. Numerous studies focus on the photonic implementations on the neural excitability of the action-potential-signaling mechanism, such as by lasers with saturable absorber or optical injection [6, 7]. Evidenced by biological neural networks, there are mainly two mechanisms for neurons to contact with others, the graded potential and the action potential [8]. The action potential of a spiking neuron is constant in amplitude as an all-or-none response, while the amplitude of the graded potential depends on the input intensity exemplified by the excitatory postsynaptic potential (EPSP) [9]. As a result, it is comprehensible that the graded potential can convey more information in a given period than the action potential owing to its continuously varying nature [10]. However, it is not suitable for long-distance transmission

* Corresponding author (email: wzou@sjtu.edu.cn)

for the sensitivity to noise. As the features of the graded-potential-signaling neurons, the responsivity and exponentially-decaying rate dominate the communication with neighbor neurons [11]. Currently, few studies focus on the photonic neuron employing graded potential and its processing functions.

In this paper, we study the properties of temporal integration and pulse facilitation in a distributed feedback laser diode (DFB-LD). Its dynamics in response to different input conditions is investigated by rate equations. We theoretically and experimentally demonstrate the applications to neuromorphic information processing with DFB-LDs, including the pattern recognition, the spike timing dependent plasticity (STDP) implementation, and the sound azimuth measurement. It is noted that the STDP implementation with a DFB-LD is based on one wavelength, needless of wavelength conversion or optical filters compared with other methods [12–15].

2 Principle and simulation

The dynamics of a DFB-LD is governed by rate equations, revealing the interaction between the carrier density and the photon density. The parameter values used in the simulation are comparable to those in [16]. We apply different input conditions for studies of the graded-potential-signaling-based properties and neuromorphic processing applications with DFB-LDs. The input can be expressed as

$$I(t) = a_1 \cdot g(t-\tau_1) + a_2 \cdot g(t-\tau_2) + a_3 \cdot g(t-\tau_3), \tag{1}$$

where $g(t)$ is the Gaussian-like pulse function. a and τ represent the amplitude and the center moment, respectively. The DFB-LD features graded output when a and τ vary.

As demonstrated in [17], the graded-potential-signaling property is basically observed by a single input pulse with varying amplitudes. For the temporal integration and pulse facilitation properties, they can be explored via multiple input pulses with the same amplitude. The time interval is shorter than the relaxation time of the DFB-LD for the accumulation behavior of the excited carrier. The temporal integration property enables a neuron to accumulate the input pulses that are temporally close enough [18]. The pulse facilitation is a property that enhances the response to the input pulse when it closely follows a previous one [19]. Note that the time interval for observing the temporal integration property is shorter than that for the pulse facilitation property. Besides, the spatiotemporal pattern carries both the spatial information by the amplitudes of pulses and the temporal information by the order of pulses [20]. Pattern recognition is a basic ability for a neuromorphic photonic network [21].

STDP is a form of synaptic plasticity in biology, which models the potentiation or depression of the synaptic weight (denoted as Δw) by the time interval between the presynaptic pulse and postsynaptic pulse (denoted as $\Delta t = t_{\rm post} - t_{\rm pre}$) [22]. The Δw can be expressed as [22]

$$\Delta w = \begin{cases} A^{+}\mathrm{e}^{(-\Delta t/\tau^{+})}, \ \Delta t > 0, \\ -A^{-}\mathrm{e}^{(\Delta t/\tau^{-})}, \ \Delta t < 0, \end{cases} \tag{2}$$

where A^{+} (A^{-}) and τ^{+} (τ^{-}) are the amplitude and time constant of the potentiation (depression) process, respectively. Here we propose a single-wavelength implementation of STDP by a DFB-LD, needless of extra wavelength conversion or optical filters compared with other methods [12–15]. The presynaptic pulse and postsynaptic pulse are received by a DFB-LD with a weight denoted as $w_{\rm pre}$ and $w_{\rm post}$, respectively. Note that $w_{\rm pre}$ is set to be smaller than $w_{\rm post}$. In the case of $\Delta t > 0$ ($\Delta t < 0$), the largest peak (peak difference) of the output is used for deriving the positive (negative) Δw. In response to random input cases (i.e., $\Delta t > 0$ or $\Delta t < 0$), the STDP implementation by a DFB-LD is capable of determining the correct Δw.

Two DFB-LDs are employed in an ear-mimicking scheme for the sound azimuth measurement. While the architecture of the sound azimuth measurement scheme is inspired by [21, 23], we employ DFB-LD for faster operation time scale from millisecond to microsecond. Two DFB-LDs receive the pulses from the left ear and the right ear with a complementary weight distribution (i.e., w_1/w_2 for left-ear pulse

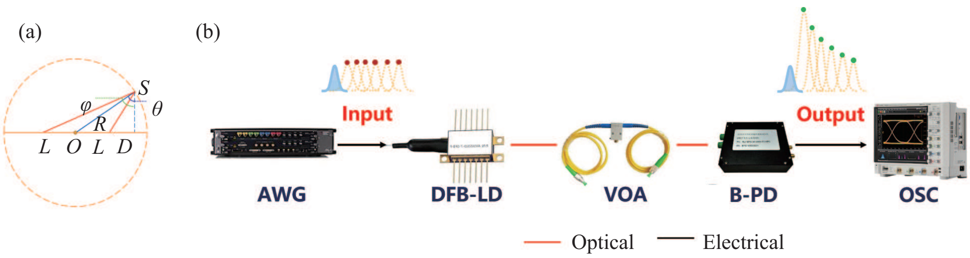

Figure 1 (Color online) (a) The analytical model for the sound azimuth measurement. S and O are the sound source and the center point, respectively. θ is the sound azimuth. L represents the distance between ears and center point. R is the distance from S to O. φ and D are intermediate variables. (b) Experimental setup for the graded-potential-signaling-based properties and neuromorphic processing applications with DFB-LDs. AWG: arbitrary waveform generator; DFB-LD: distributed feedback laser diode; VOA: variable optical attenuator; B-PD: balanced photodetector; OSC: oscilloscope.

and w_2/w_1 for right-ear pulse). The time interval between the pulses implies the clue for sound azimuth, which is the receiving delay between the left and right ears (denoted as Rd) (see Figure 1(a) for the analytical model). We make use of exponentially-decaying function to model the output of a DFB-LD to $g(t)$. The output difference between two DFB-LDs at the time when the second pulse arrives can be described as

$$\Delta S = w_1 \cdot S_0 \cdot (\mathrm{e}^{-\alpha\cdot\mathrm{Rd}} - 1) + w_2 \cdot S_0 \cdot (1 - \mathrm{e}^{-\alpha\cdot\mathrm{Rd}}), \tag{3}$$

where S_0 and α are the amplitude and decaying rate, respectively. In a consequence, we can obtain the sound azimuth information by the measurement of ΔS. Recently, a scheme of the sound azimuth measurement is demonstrated by the VCSEL-SA-based photonic spiking neuron [24]. In addition to this similar architecture adopted, the distinct encoding and decoding schemes result in a spike-timing-difference indication of the sound azimuth, different from the ΔS we use. As the foregoing discussion, the graded-potential-based scheme is more susceptible to the amplitude noise with decreased measurement accuracy. However, in an acceptable range of noise and accuracy, the DFB-LD-based scheme may provide an easily-accessible and low-cost solution.

The experimental setup for the graded-potential-signaling-based properties and neuromorphic processing applications with DFB-LDs is shown in Figure 1(b). Note that the setup for sound azimuth measurement is to double the original one. The input is provided by an arbitrary waveform generator (AWG, Keysight M8195A). A DFB-LD (Emcore-Ortel, 1751A-35-BB-FC-10) is driven by a laser diode controller (Thorlabs, lTC4001) with an external modulation bandwidth of 150 kHz. Subsequently, a variable optical attenuator (VOA) is adopted to adjust the input optical power of a pair of balanced photodetectors (B-PD, fsphotonics, FS-PD-B-2030). At the end, an oscilloscope (Keysight, DSO-S 804A) monitors the output in the electrical domain.

By rate equations, we simulate the graded-potential-signaling-based properties and neuromorphic processing applications with DFB-LDs at a bias current of 15 mA. It is mentioned that the full-width-at-half-maximum (FWHM) of $g(t)$ is 1 μs. The results are presented in Figure 2. In Figure 2(a), a_1 is set to be 0.1, 0.5, and 1, respectively. The carrier density and photon density both rise in a graded manner. Besides, the slope of the rising front of the photon density also increases with a_1. The temporal integration property is given in Figure 2(b). The three input pulses are temporally integrated by a DFB-LD in the conditions of $\tau_2 - \tau_1 = \tau_3 - \tau_2 = \tau = 1$ μs and $a_1 = a_2 = a_3 = 0.1$. It leads to a stronger response of the photon density. As shown in Figure 2(c), τ increases to 1.5 μs. The pulse facilitation property is observed that the responses to latter input pulses are strengthened owing to the previous input pulse. It supports the pattern recognition ability presented in Figure 2(d), where a_1:a_2:a_3 is 5:2:1 or 1:2:5 as two spatiotemporal patterns with τ of 1 μs. One pattern (lower panel) leads to a response of the DFB-LD while the other (upper panel) cannot. Owing to the facilitation provided by previous pulses, the third pulse causes a greater response of photon density than that in the other case. As a conclusion, the DFB-LD is sensitive to the order of the input pulses.

The simulation result of the STDP implementation is indicated in Figure 2(e). The presynaptic pulse and the postsynaptic pulse are generated with varying Δt and a w_{pre}:w_{post} of 1:5. We measure the largest

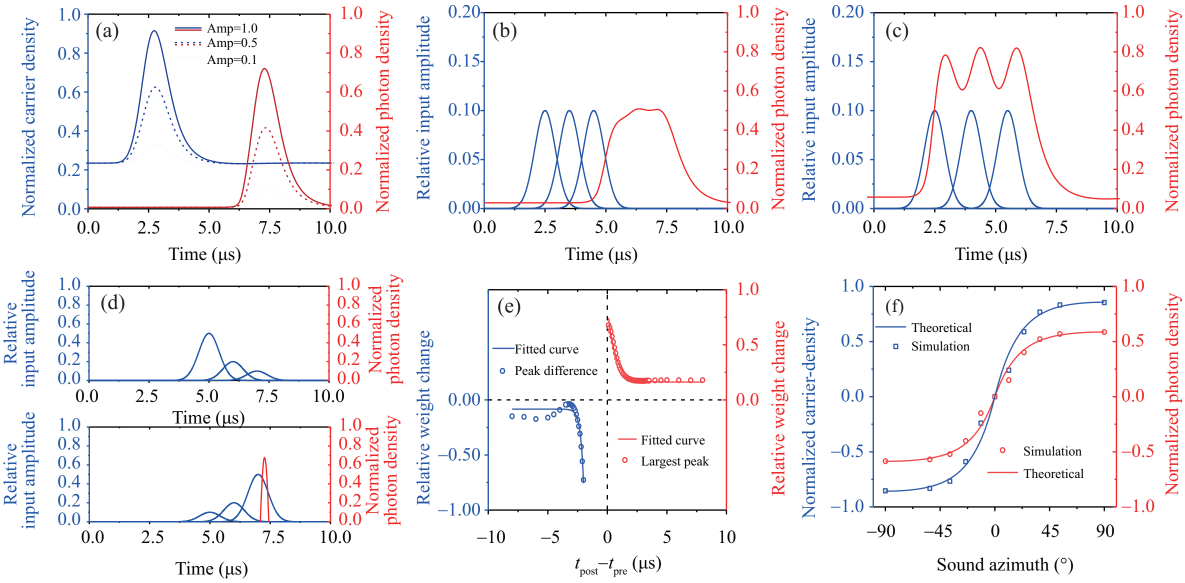

Figure 2 (Color online) Simulation results of the graded-potential-signaling-based properties and neuromorphic processing applications with DFB-LDs. The properties of the graded-potential-signaling (a), the temporal integration (b), and the pulse facilitation (c). The neuromorphic processing applications of the pattern recognition (d), the STDP implementation (e), and the sound azimuth measurement (f).

peak (peak difference) of the output for potentiation (depression) process. The fitted curve is plotted for theoretical reference as given in (2), which is matched well by the result of STDP implementation. The sound azimuth measurement is simulated and presented in Figure 2(f). We test the responses of two DFB-LDs to the left-ear pulse and right-ear pulse with different Rd and a w_1:w_2 of 1:5. ΔS of the photon density and the carrier density are both recorded. Besides, the theoretical curve is given by (3). It is worth noting that the results by rate equations agree with the theoretical curve in a good consistency. Consequently, the sound azimuth can be measured by ΔS.

3 Experimental results

3.1 Properties of graded-potential-signaling, pulse facilitation, and temporal integration

For the observation of the graded-potential-signaling property, we adjust a_1 for $g(t)$ with 1 µs FWHM as shown in Figure 3(a). Apparently, the DFB-LD features the graded output pulse. It is found that the peak-to-peak delay between the input pulse and output pulse decreases with a_1. Figure 3(b) presents the output pulse to an 80-mV input pulse with 15 mA bias current. The consistency between the experimental result and the exponentially-decaying fitted result verifies (3). Subsequently, we generate three 210-mV input pulses with 1 µs FWHM and varying τ of 6 µs, 2.5 µs, and 1.5 µs as indicated by Figures 3(c)–(e), respectively. In Figure 3(c), each of the input pulses independently induces an identical output pulse. When τ is reduced to 2.5 µs in Figure 3(d), the output pulses merge. Note that the peak of the first output pulse is lower than that of the latter two output pulses. It reflects that the latter output pulses are facilitated because of the pervious input pulse, demonstrating the pulse facilitation property. As illustrated by Figure 3(e), when the input pulses become closer, the peaks of the output pulses get indistinguishable. The input pulses accumulate to cause a larger output pulse. Accordingly, the temporal integration property is observed. It is noteworthy that the pump trace in Figure 3(c)–(e) is monitored by the R6 port on the rear panel of the laser diode controller.

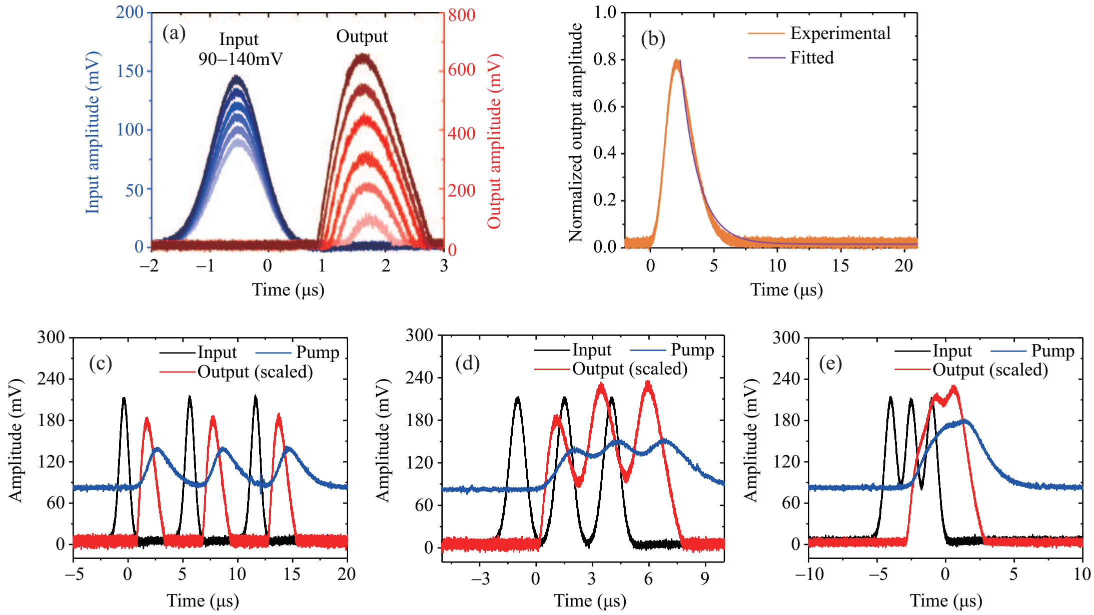

Figure 3 (Color online) Experimental results of the graded-potential-signaling-based properties with DFB-LDs. (a) The graded-potential-signaling property. (b) An output pulse compared with the exponentially-decaying fitted curve. (c)–(e) Responses of a DFB-LD to three input pulses with τ of 6 μs, 2.5 μs (for pulse facilitation property), and 1.5 μs (for temporal integration property), respectively.

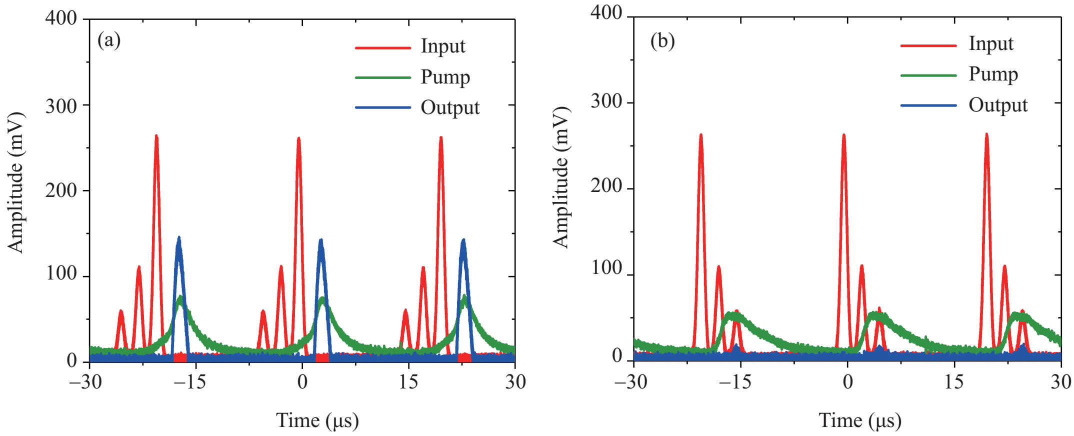

Figure 4 (Color online) The response of a DFB-LD to the sequential input pattern (a) and the input pattern in reverse order (b).

3.2 Neuromorphic processing applications of pattern recognition, STDP implementation, and sound azimuth measurement

The pattern recognition ability of a DFB-LD is tested as shown in Figure 4. The sequential input pattern consists of three pulses separated by 2.5 μs with an amplitude of 50 mV, 100 mV, and 250 mV, respectively. As displayed by Figure 4(a), the sequential input pattern can induce a greater response of the DFB-LD, indicating that it can be recognized. In Figure 4(b), there is hardly response to the input pattern in reverse order, standing for the unsuccessful recognition. The amplitude of pump current in Figure 4(a) is larger than that in Figure 4(b). It is because the response to the last pulse of the sequential input pattern is facilitated by the previous pulses. However, this facilitation effect is absent for the input pattern in reverse order, making the DFB-LD silent.

The results of the STDP implementation by a DFB-LD are presented in Figure 5. With a 125 mV

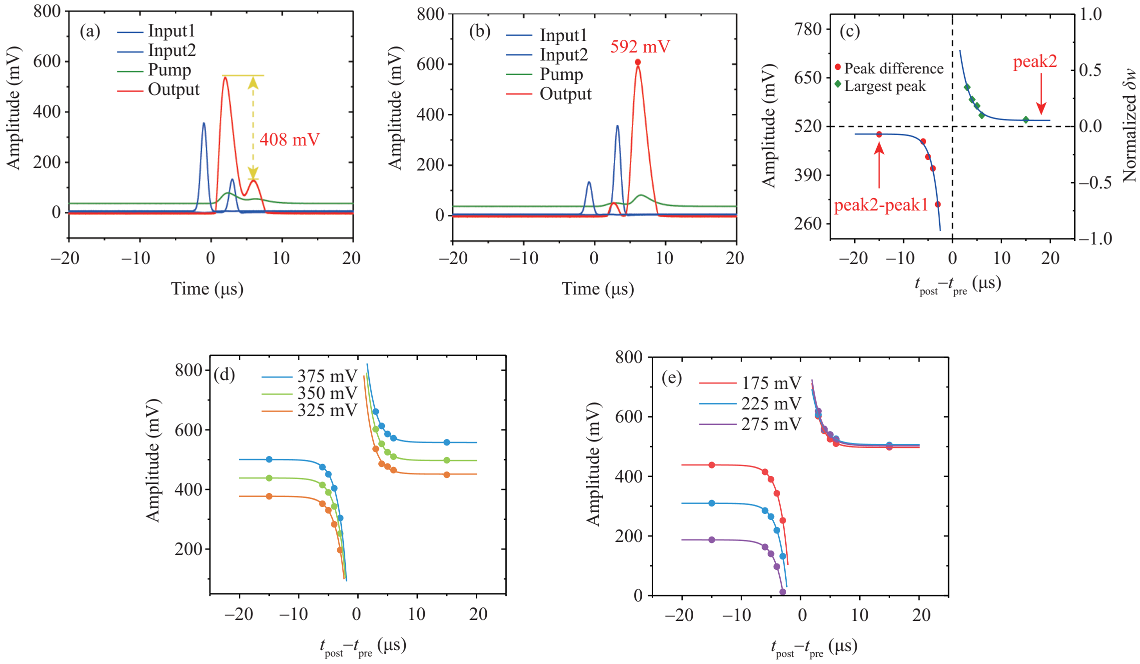

Figure 5 (Color online) The experimental results of the STDP implementation by a DFB-LD. The output at (a) $\Delta t = -4$ μs and (b) $\Delta t = 4$ μs. (c) The peak difference and the largest peak dependent on Δt corresponding to the STDP curve. The effects on the STDP curve of varying (d) $w_{\rm post}$ and (e) $w_{\rm pre}$.

(350 mV) presynaptic (postsynaptic) pulse, the DFB-LD exhibits different outputs when Δt is -4 μs (Figure 5(a)) and 4 μs (Figure 5(b)), respectively. In Figure 5(c), we plot the peak difference and the largest peak corresponding to different Δt. When the pulses grow apart, the peak difference increases to a limitation (denoted as peak2-peak1), and the largest peak decays to a limitation (denoted as peak2). Meanwhile, the measured STDP curve is given. We find that the experimental results match well with the theoretical STDP curve governed by (2). Performed by Figures 5(d) and (e), we investigate the effects of $w_{\rm post}$ and $w_{\rm pre}$ on the measured STDP curve, respectively. In Figure 5(d), the level of the measured STDP curve rises with $w_{\rm post}$. In Figure 5(e), as $w_{\rm pre}$ increases, the potentiation part is approximately steady while the depression part degrades. In conclusion, the STDP curve can be adjusted by applied parameters.

The experimental results of the sound azimuth measurement are shown in Figure 6. In the condition of a 350 mV (70 mV) input pulse corresponding to w_2 (w_1), we measure ΔS (i.e., 2nd peak difference) when Rd = 3 μs (Figure 6(a)) and Rd = 4 μs (Figure 6(b)), respectively. Also, ΔS dependent on Rd is obtained and is then compared with the theoretical curve modeled by (3), showing a good agreement in Figure 6(c). After the transformation from Rd into the sound azimuth, the sound azimuth can be determined by ΔS in Figure 6(d). Consequently, the scheme of sound azimuth measurement by two DFB-LDs is experimentally demonstrated.

4 Conclusion

We have demonstrated theoretically and experimentally that a commonly-used DFB-LD can work as a graded-potential-signaling photonic neuron. The temporal integration and pulse facilitation properties of the DFB-LD are investigated. Additionally, applications to neuromorphic information processing of the pattern recognition, the STDP implementation, and the sound azimuth measurement based on DFB-LDs are presented. Future work will focus on the potentially-integrated pattern recognition network using DFB-LDs [25]. For a given target pattern, the DFB-LD-based STDP module derives the Δw that is inversely proportional to the timing difference between the spike and the teacher signal in the

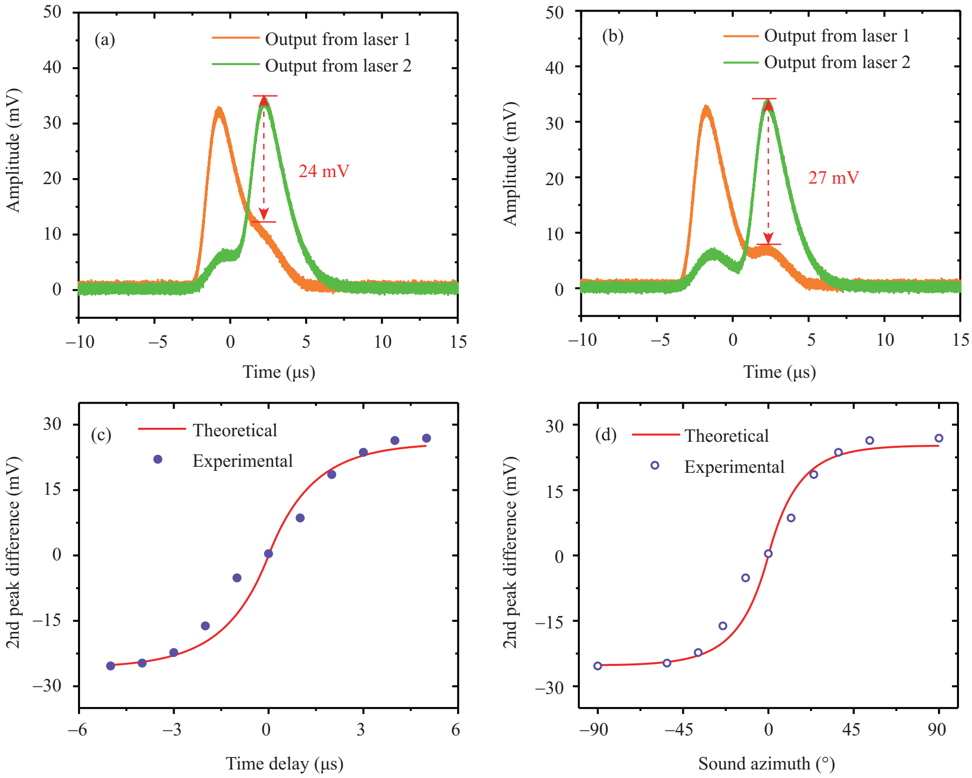

Figure 6 (Color online) The experimental results of the sound azimuth measurement with DFB-LDs. The output when (a) Rd = 3 μs and (b) Rd = 4 μs. The ΔS dependent on (c) the Rd and (d) the sound azimuth.

corresponding branch. Thus, the weight can be updated properly employing Δw as an indication.

Acknowledgements This work was supported by National Key R&D Program of China (Grant No. 2019YFB2203700) and National Natural Science Foundation of China (Grant No. 61822508).

References

1 Peng H T, Nahmias M A, de Lima T F, et al. Neuromorphic photonic integrated circuits. IEEE J Sel Top Quantum Electron, 2018, 24: 1–15
2 Prucnal P R, Shastri B J. Neuromorphic Photonics. Boca Raton: CRC Press, 2017
3 Rajamani V, Kim H, Chua L. Morris-Lecar model of third-order barnacle muscle fiber is made of volatile memristors. Sci China Inf Sci, 2018, 61: 060426
4 Yang C J, Adhikari S P, Kim H S. Excitatory and inhibitory actions of a memristor bridge synapse. Sci China Inf Sci, 2018, 61: 060427
5 Li Y, Zhou Y X, Wang Z R, et al. Memcomputing: fusion of memory and computing. Sci China Inf Sci, 2018, 61: 060424
6 Prucnal P R, Shastri B J, de Lima T F, et al. Recent progress in semiconductor excitable lasers for photonic spike processing. Adv Opt Photon, 2016, 8: 228–299
7 Robertson J, Wade E, Hurtado A. Electrically controlled neuron-like spiking regimes in vertical-cavity surface-emitting lasers at ultrafast rates. IEEE J Sel Top Quantum Electron, 2019, 25: 1–7
8 Jiang P, Chen C, Liu X B, et al. Generation and characterization of spiking and nonspiking oligodendroglial progenitor cells from embryonic stem cells. Stem Cells, 2013, 31: 2620–2631
9 Eyal G, Verhoog M B, Testa-Silva G, et al. Human cortical pyramidal neurons: from spines to spikes via models. Front Cell Neurosci, 2018, 12: 181
10 DiCaprio R A. Information transfer rate of nonspiking afferent neurons in the crab. J Neurophysiol, 2004, 92: 302–310
11 Li Z, Liu J, Zheng M, et al. Encoding of both analog- and digital-like behavioral outputs by one C. elegans interneuron. Cell, 2014, 159: 751–765
12 Xiang S Y, Zhang Y H, Gong J K, et al. STDP-based unsupervised spike pattern learning in a photonic spiking neural network with VCSELs and VCSOAs. IEEE J Sel Top Quant, 2019, 25: 1700109
13 Ren Q S, Zhang Y L, Wang R, et al. Optical spike-timing-dependent plasticity with weight-dependent learning window and reward modulation. Opt Express, 2015, 23: 25247–25258
14 Toole R, Tait A N, de Lima T F, et al. Photonic implementation of spike-timing-dependent plasticity and learning

algorithms of biological neural systems. J Lightw Technol, 2016, 34: 470–476
15 Fok M P, Tian Y, Rosenbluth D, et al. Pulse lead/lag timing detection for adaptive feedback and control based on optical spike-timing-dependent plasticity. Opt Lett, 2013, 38: 419–421
16 Zhang J, Gao C X, Xue M Y, et al. Research on frequency modulation character of the current driven DFB semiconductor laser. Mod Phys Lett B, 2019, 33: 1850422
17 Liu Q, Hollopeter G, Jorgensen E M. Graded synaptic transmission at the Caenorhabditis elegans neuromuscular junction. Proc Natl Acad Sci USA, 2009, 106: 10823–10828
18 Selmi F, Braive R, Beaudoin G, et al. Temporal summation in a neuromimetic micropillar laser. Opt Lett, 2015, 40: 5690–5693
19 Zucker R S, Regehr W G. Short-term synaptic plasticity. Annu Rev Physiol, 2002, 64: 355–405
20 Hu J, Tang H J, Tan K C, et al. How the brain formulates memory: a spatio-temporal model research frontier. IEEE Comput Intell Mag, 2016, 11: 56–68
21 Wang W, Pedretti G, Milo V, et al. Learning of spatiotemporal patterns in a spiking neural network with resistive switching synapses. Sci Adv, 2018, 4: eaat4752
22 Froemke R C, Dan Y. Spike-timing-dependent synaptic modification induced by natural spike trains. Nature, 2002, 416: 433–438
23 He Y L, Nie S, Liu R, et al. Spatiotemporal information processing emulated by multiterminal neuro-transistor networks. Adv Mater, 2019, 31: 1900903
24 Song Z W, Xiang S Y, Ren Z X, et al. Photonic spiking neural network based on excitable VCSELs-SA for sound azimuth detection. Opt Express, 2020, 28: 1561–1573
25 Ma B W, Chen J P, Zou W W. A DFB-LD-based photonic neuromorphic network for spatiotemporal pattern recognition. In: Proceedings of Optical Fiber Communication Conference, San Diego, 2020. M2K.2